Comparison of local, semi-microscopic, and microscopic three-cluster models

M. Theeten,[1,2,*] D. Baye,[1,2,†] and P. Descouvemont[2,‡]
[1]*Physique Quantique, C.P. 165/82, Université Libre de Bruxelles, B 1050 Brussels, Belgium*
[2]*Physique Nucléaire Théorique et Physique Mathématique, C.P. 229, Université Libre de Bruxelles, B 1050 Brussels, Belgium*
(Received 17 June 2006; published 10 October 2006)

Two different three-body models are compared with a fully antisymmetrized microscopic three-cluster model. The local model makes use of local effective interactions involving forbidden states among the three particles. In the semi-microscopic model, nonlocal two-body interactions are derived within the resonating-group method from the same nucleon-nucleon effective forces as in the microscopic model. In both cases, calculations are performed in hyperspherical coordinates with the Lagrange-mesh method. The role of forbidden states and their elimination are discussed. The models are applied to an $\alpha\alpha n$ description of ^{9}Be and an αnn description of ^{6}He. The local model results are affected by almost forbidden states and may be unrealistic for ^{9}Be. A comparison of the microscopic and semi-microscopic models shows that the effect of exchanges involving the three clusters is weak. An overbinding of ^{9}Be cannot be avoided with nucleon-nucleon forces reproducing αn and $\alpha\alpha$ scattering properties. On the contrary, ^{6}He is underbound under the same conditions. This can probably be attributed to a lack of three-nucleon forces.

DOI: 10.1103/PhysRevC.74.044304 PACS number(s): 21.60.Gx, 21.45.+v, 27.20.+n

I. INTRODUCTION

Some nuclei present a multicluster structure, i.e., nucleons appear to gather into well-bound entities called clusters, the binding between those clusters being weaker than their internal cohesion [1–3]. The best cluster candidate is the α cluster composed of two protons and two neutrons, because of the large binding energy of the α particle.

Although the existence of a cluster structure for a number of light nuclei conforts physical intuition, the nature of the clusters and of their interaction is undoutbly much more complicated than it may seem at first sight. Because of the indiscernibility of nucleons, it is not possible to say which nucleons belong to a cluster. The precise contents of a cluster is thus not well defined inside a nucleus. Accordingly, the interaction between clusters is also difficult to define. It may be very complicated and, in particular, nonlocal.

The simple point-cluster model with local forces (hereafter denoted as local model) has been applied to some light nuclei [4–8]. Most early calculations concerned the 3α system and were based on shallow $\alpha\alpha$ potentials. As they did not agree well with experiment, it was argued that shallow potentials do not simulate the nonlocality of the cluster-cluster interaction. The effect of nonlocality can be simulated with deep potentials possessing unphysical "forbidden" states. These forbidden states can be ignored in two-body systems but must be eliminated in multicluster models [6,9]. Studies of the 3α system show a strong sensitivity to the technique of elimination [6,10,11] that has only recently received an explanation [12,13]: the presence or absence of some almost forbidden states strongly affects the energy.

In parallel to that model, the microscopic cluster model where all nucleons are taken into account and Pauli antisymmetrization is treated exactly has met considerable success for the spectroscopy of light nuclei as well as for reactions between them [14–17]. Three-cluster microscopic models have been used for some time but their treatment has recently been improved by combining them with the hyperspherical formalism [18]. The ^{12}C nucleus is well described by a 3α *microscopic* model [14,15] but its results are not easily comparable with those of the local model [11].

An intermediate model has been developed by Fujiwara and coworkers for three clusters that in this article is termed "semi-microscopic" model [19,20]. It resembles a point-cluster model but for the use of microscopically founded cluster-cluster interactions derived from a microscopic two-cluster model known as the resonating-group method (RGM) [1]. Such interactions are nonlocal. Hence two-cluster aspects of antisymmetrization are simulated in this model, i.e., all nucleon exchanges between each pair of clusters, but triple exchanges are ignored, i.e., nucleon exchanges involving all three clusters. In the approach of Refs. [19,20], calculations are performed in momentum space with the Faddeev equation, where the nonlocality of the forces is handled easily. The Coulomb forces require a special treatment.

This model is more realistic than the local model and simpler than the microscopic model. We think that its main merit is to provide a more physical understanding of the similarities and differences between structureless-cluster models and microscopic cluster models. The main goal of the present work is to perform such a comparison.

During the previous years, in addition to the microscopic three-cluster model, our group has developed techniques for accurately solving three-body Schrödinger equations, first with local forces [8] and then with nonlocal forces [21]. More precisely, we have developed a technique for treating three-cluster systems with nonlocal forces in configuration space [21]. The wave functions and energies are calculated

*Electronic address: mtheeten@ulb.ac.be
†Electronic address: dbaye@ulb.ac.be
‡Electronic address: pdesc@ulb.ac.be

with the Lagange-mesh technique, an approximate variational calculation strongly simplified by the use of a Gaussian quadrature [22,23]. This approach is (relatively) simple, fast, and accurate. The treatment of Coulomb forces between clusters raises no difficulties. The local case has already been extended to studying the continuum [24].

In the present work, we perform a comparison of the local, semi-microscopic, and microscopic cluster models to analyze their properties, determine their limitations and, mainly, to have a better understanding of their validity for nuclei with such a structure. The models are applied to an $\alpha\alpha n$ description of ^{9}Be and an αnn description of ^{6}He.

In Sec. II, the microscopic two-cluster model is summarized and the nonlocal interaction between the clusters is defined. In Sec. III, a short presentation of the different three-cluster models is done. The elimination of forbidden states is considered in Sec. IV. Results are presented and discussed in Sec. V. Section VI is devoted to concluding remarks.

II. TWO-CLUSTER RESONATING GROUP METHOD

A. RGM equation

The microscopic Hamiltonian h_A of a nucleus involving A nucleons can be written as

$$h_A = \sum_{i=1}^{A} t_i + \sum_{i>j=1}^{A} v_{ij}, \tag{1}$$

where t_i is the kinetic-energy operator of nucleon i and v_{ij} is an effective interaction between nucleons i and j, including spin-orbit and Coulomb forces. In the RGM, one searches for approximate solutions of the Schrödinger equation

$$h_A\psi = E_A\psi, \tag{2}$$

where E_A is the total energy of the nucleus.

Let us consider in this section a system of A nucleons separated into two clusters containing A_1 and A_2 nucleons. In the RGM [1,2], this system is approximately described for each partial wave by a microscopic wave function defined as

$$\psi_{lS}^{JM\pi} = \mathcal{A}[[\phi_1 \otimes \phi_2]^S \otimes Y_l(\Omega)]^{JM} r^{-1} g_{lS}^J(r), \tag{3}$$

where $\mathcal{A}$ is the nucleon antisymmetrization projector; $\boldsymbol{r} = (r, \Omega)$ is the coordinate between the cluster centers of mass; and l, S, J, and π are, respectively, the relative-motion orbital momentum, the total spin, the total angular momentum, and the parity of the nucleus. The center-of-mass motion is described by a plane wave that is not displayed here. The wave function $g_{lS}^J(r)$ of the relative motion of the clusters is the only unknown function to be determined in Eq. (3). In the RGM, one indeed assumes that the internal wave functions ϕ_i $(i = 1, 2)$ are approximated in the translation-invariant harmonic-oscillator shell model as

$$\phi_i = \exp\left[-\frac{1}{2b^2}\sum_{j=1}^{A_i}\left(\boldsymbol{r}_j^{(i)} - \boldsymbol{R}_i\right)^2\right]\chi_i, \tag{4}$$

where b is a common oscillator parameter for both clusters, A_i is the number of nucleons that make up cluster i, $\boldsymbol{r}_j^{(i)}$ is the coordinate of the jth nucleon of cluster i, and $\boldsymbol{R}_i$ is the coordinate of its center of mass. Spinor χ_i involving the spin-isospin parts of the nucleon wave functions ensures the antisymmetry of ϕ_i. The internal energies of the clusters are approximated by the variational expressions

$$E_i = \langle\phi_i|h_{A_i}|\phi_i\rangle. \tag{5}$$

To simplify the presentation, we drop the spins in the rest of this section.

Using the microscopic wave function (3) as an approximate solution of the Schrödinger equation (2), the RGM leads to a nonlocal Schrödinger equation for the relative motion [1],

$$-\frac{\hbar^2}{2\mu}\left[\frac{d^2}{dr^2} - \frac{l(l+1)}{r^2}\right] + V_D(r)g_l(r) + \int_0^\infty k_l(\varepsilon, r, r')g_l(r')\,dr' = \varepsilon g_l(r), \tag{6}$$

where μ is the reduced mass of the two clusters and

$$\varepsilon = E_A - E_1 - E_2 \tag{7}$$

is the energy of the relative motion between the clusters. This equation shows that an effective nonlocal potential acts between the clusters. Its local part V_D is usually called the direct potential. The nonlocal part of the interaction contains for each partial wave a kernel $k_l(\varepsilon, r, r')$ that depends on the relative energy ε of the system. This property is a consequence of exchanges of nucleons between the clusters, which arise from the antisymmetrization operator $\mathcal{A}$. The dependence of $k_l(\varepsilon, r, r')$ on ε is linear,

$$k_l(\varepsilon, r, r') = k_{Hl}(r, r') + \varepsilon\, k_{Nl}(r, r'), \tag{8}$$

where k_{Hl} and k_{Nl} are the Hamiltonian and norm kernels, respectively. Explicit expressions of kernels are displayed in Appendix A for the $\alpha + n$ and $\alpha + \alpha$ systems. Spin effects can be observed in the $\alpha + n$ case.

B. Effective interaction between clusters

The RGM equation can be interpreted as defining an effective interaction V between two clusters according to the relative-motion equation

$$(T + V)\Psi = \varepsilon\Psi, \tag{9}$$

where T is the relative kinetic energy of the clusters. This equation reads more explicitly

$$\left[-\frac{\hbar^2}{2\mu}\Delta + V_D(r)\right]\Psi(\boldsymbol{r}) + \int K(\varepsilon, \boldsymbol{r}, \boldsymbol{r}')\Psi(\boldsymbol{r}')d\boldsymbol{r}' = \varepsilon\Psi(\boldsymbol{r}), \tag{10}$$

where the nonlocal kernel is defined by

$$K(\varepsilon, \boldsymbol{r}, \boldsymbol{r}') = (rr')^{-1}\sum_{lm} Y_l^{m*}(\Omega)Y_l^m(\Omega')k_l(\varepsilon, r, r'). \tag{11}$$

The interaction V between the clusters thus contains a local part V_D and a nonlocal part with kernel K. The nonlocal term always depends on angular momentum. The local term may (αn) or may not $(\alpha\alpha)$ depend on it (see Appendix A).

C. Forbidden states

For a given partial wave, by moving the part of k_l proportional to ε to the right-hand side, the Schrödinger equation (6) can be rewritten formally as

$$\mathcal{H}_l g_l = \varepsilon \mathcal{N}_l g_l, \tag{12}$$

where $\mathcal{H}_l$ and $\mathcal{N}_l$ are operators that are independent of ε.

When the microscopic wave functions (3) exactly vanish

$$\mathcal{A}\left[\phi_1\phi_2 Y_l^m(\Omega) r^{-1} g_l^{\rm FS}(r)\right] = 0, \tag{13}$$

for nonvanishing functions $g_l^{\rm FS}$, these functions $g_l^{\rm FS}$ are clearly unphysical and are known as *Pauli forbidden states* of the relative motion of the two clusters.

Forbidden states correspond to zero eigenvalues of operators $\mathcal{H}_l$ and $\mathcal{N}_l$,

$$\mathcal{H}_l g_l^{\rm FS} = 0, \tag{14}$$

$$\mathcal{N}_l g_l^{\rm FS} = 0. \tag{15}$$

The eigenfunctions $g_l^{\rm FS}$ satisfy Eqs. (12) and (6) for any value of ε.

III. THREE-BODY MODELS

A. Local three-body models

In the local model, the nucleus is considered to be composed of three structureless particles or clusters interacting through local two-body interactions. These phenomenological interactions are usually derived from scattering properties of the physical nuclei corresponding to the interacting clusters [8] or inspired from a nuclear model [25]. In other words, the internal structures of the clusters and the interaction between each pair of clusters is assumed to be unaffected by the presence of a third cluster. The forces may support some additional unphysical states to simulate effects of the Pauli principle between nucleons. Although we call it local, the model may contain some amount of nonlocality: (i) interactions may depend on the angular momentum and (ii) the elimination of forbidden states may involve nonlocal projection operators.

Let us distribute the A nucleons of a nucleus into three clusters with mass numbers A_i such that $A_1 + A_2 + A_3 = A$. Assuming two-body forces only, the Schrödinger equation of the system can be written as

$$\left(\sum_{k=1}^{3} T_k + \sum_{i>j=1}^{3} V_{ij}\right) \Psi^{JM\pi} = E\Psi^{JM\pi}, \tag{16}$$

where T_k is the kinetic energy of cluster k, V_{ij} is the potential between clusters i and j, and E is the total energy of the cluster relative motions. The wave function $\Psi^{JM\pi}$ depends on two internal coordinates of the system as well as on the total angular momentum J, its projection M, and the parity π of the three-body relative motion.

As in our previous works [8,21], we make use of hyperspherical coordinates. The wave function is expanded in hyperspherical harmonics as

$$\Psi^{JM\pi}(\rho, \Omega_5) = \rho^{-5/2} \sum_{\gamma K} \chi_{\gamma K}^{J\pi}(\rho) \mathcal{Y}_{\gamma K}^{JM}(\Omega_5), \tag{17}$$

where ρ is the hyperradius, Ω_5 represents the five angular variables, and $\mathcal{Y}_{\gamma K}^{JM}(\Omega_5)$ are hyperspherical harmonics. Index K is the hypermomentum and index γ stands for different orbital momenta and spins. See Ref. [8] and references therein for details.

We apply the Lagrange-mesh technique [22,23] to solve Eq. (16). In this approach, a set of N functions $\hat{f}_i(u)$ is associated with a set of N mesh points u_i in such a way that each Lagrange function $\hat{f}_i$ vanishes at all mesh points but u_i. The hat in $\hat{f}_i$ indicates that the functions are properly regularized [8,23]. The mesh points correspond to the zeros of a Gauss-Laguerre quadrature. The hyperradial partial wave functions $\chi_{\gamma K}^{J\pi}$ are expanded over the set of Lagrange functions as [8]

$$\chi_{\gamma K}^{J\pi}(\rho) = h^{-1/2} \sum_{i=1}^{N} c_{\gamma K i}^{J\pi} \hat{f}_i(\rho/h), \tag{18}$$

where h is a scaling factor aimed at adapting the mesh to the physical extension of the system and the $c_{\gamma K i}^{J\pi}$ are variational coefficients. An important simplification occurs in the calculation because of the use of the Gauss quadrature associated with the mesh. The variational equations take the form of mesh equations without loss of accuracy [8,23].

B. Semi-microcopic three-body models

The semi-microscopic model is very similar to the local model except that it makes use of two-body interactions derived from the RGM rather than from phenomenological interactions [19,20]. The nonlocal effective potential between a pair of clusters is defined from the two-cluster RGM equation (9). We use these potentials in three-body systems described with the same Eq. (16) as in the local model. In that case, expansions (17) and (18) remain valid. The only change is that the potentials V_{ij} become nonlocal,

$$V_{ij}\Psi^{JM\pi} = V_{Dij}(\boldsymbol{r}_{ij})\Psi^{JM\pi} + \int d\boldsymbol{r}'_{ij} K_{ij}(\varepsilon, \boldsymbol{r}_{ij}, \boldsymbol{r}'_{ij})\Psi^{JM\pi}, \tag{19}$$

where $\boldsymbol{r}_{ij} = \boldsymbol{r}_i - \boldsymbol{r}_j$ is the relative coordinate between clusters i and j. We then solve the equation with the Lagrange-mesh technique, which we have already extended to nonlocal interactions [21].

RGM potentials are more physical because they are directly derived from nucleon-nucleon interactions and verify the Pauli antisymmetrization between a pair of clusters. However, they depend on angular momentum and on energy. Each of these potentials depends on a parameter ε that corresponds to the energy of the relative motion of the two interacting clusters. Because these energies are not fixed in a three-body system, they appear here as parameters. This is a drawback of this model, because we have to choose their values and there is no unique way of making this choice. A possibility consists in

using an average value according to a prescription of Fujiwara *et al*. [19]. It is described and discussed in Sec. V A.

Other potentials can be defined for the semi-microscopic model but we do not consider them here as they require more difficult calculations. The two-body RGM equation (12) can be rewritten as

$$\mathcal{N}_l^{1/2}(T+\hat{V}-\varepsilon)\mathcal{N}_l^{1/2}g_l = 0. \tag{20}$$

This expression is similar to the local Eq. (9) if $\mathcal{N}_l^{1/2}g_l$ is taken as wave function [2,25–27]. It defines an effective potential $\hat{V}$ that has the advantage over the previous one that it does not depend on energy and does not have the above-mentioned drawback. The construction of this potential is formally well known but very difficult in practice. The square root of $\mathcal{N}_l$ must be calculated and its allowed part must be inverted.

A semi-microscopic three-body model based on this approach has been studied by Schmid [26] and the role of three-cluster exchanges has been approximately evaluated [28]. A general theoretical account is given in Ref. [27]. A full numerical study of this model would also be very interesting and should be attempted in the future.

C. Microscopic three-cluster models

Microscopic models are derived from basic principles of quantum mechanics, such as the treatment of all nucleons with exact antisymmetrization of the wave functions. The Hamiltonian of an A-nucleon system is given by Eq. (1) with some effective nucleon-nucleon force. Several versions of three-cluster microscopic models exist, differing by the treatment of the relative motion between the clusters [15–17]. Here we consider a recent version based on hyperspherical coordinates [18].

In the hyperspherical formalism, the total microscopic wave function is a direct extension of Eq. (17). It is defined by

$$\Psi^{JM\pi} = \sum_{\gamma K} \mathcal{A}\rho^{-5/2}\chi_{\gamma K}^{J\pi}(\rho)\mathcal{Y}_{\gamma K}^{JM}(\Omega_5) \times [\phi_1 \otimes [\phi_2 \otimes \phi_3]^{S_{23}}]^{SM_S}, \tag{21}$$

where ϕ_1, ϕ_2, ϕ_3 are the internal wave functions of the three clusters as described in Sec. II A. These internal functions depend on the internal coordinates of the clusters. An important difference from the models of Secs. III A and III B is that the hyperradius ρ and hyperangles Ω_5 are now defined as a function of the center-of-mass coordinates of the clusters and are thus functions of the A nucleon coordinates. In the local and semi-microscopic models, they depend only on the three cluster coordinates.

In a microscopic model, calculations are thus very different and we do not describe them here. The hyperradial wave functions $\chi_{\gamma K}^{J\pi}(\rho)$ are expanded in terms of shifted Gaussian functions, depending on a generator coordinate R. This makes the basis functions equivalent to projected Slater determinants. The matrix elements are computed from the numerical calculation of seven-dimension integrals (see Ref. [18] for details).

IV. REMOVAL OF PAULI FORBIDDEN STATES

A. Motivation

In the local and semi-microscopic models, forbidden states may appear in the two-cluster relative motion. In the local model, the notion of forbidden states corresponds to bound states of the two-cluster system at unphysically low energies. They occur thus for deep potentials selected to simulate the correct node structure of the physical bound states located at energies consistent with experiment. In the semi-microscopic model, as explained in Sec. II C, forbidden states are eigenfunctions with zero eigenvalue of the norm operator. They are not related with some energy.

Forbidden states can often just be ignored in two-cluster systems. This is not true for three-body systems where two-body interactions display forbidden states. They affect in an unphysical way the energies of the system. Forbidden states also exist in the three-cluster microscopic model but they do not raise problems in a fully antisymmetrized treatment.

In the local and semi-microscopic models, the effect of forbidden states must be eliminated. One imposes that the three-body wave function does not contain two-body forbidden states. For that purpose, two approaches are used that we now summarize.

B. Pseudopotential method

In the pseudopotential method [9], an operator P is defined as the sum of projectors on the forbidden states,

$$P = \sum_{i>j=1}^{3}\sum_{n=1}^{N_{ij}} |g_{n,ij}^{\mathrm{FS}}\rangle\langle g_{n,ij}^{\mathrm{FS}}|, \tag{22}$$

where N_{ij} is the number of forbidden states for the relative motion between clusters i and j, and $|g_{n,ij}^{\mathrm{FS}}\rangle$ are those forbidden states. Notice that P is not a projector although it is a sum of two-body projectors [6].

Different models lead to different types of forbidden states. In the RGM approach, the two-body forbidden states are described by harmonic-oscillator wave functions with a value $b/\sqrt{\mu_{ij}}$ of the oscillator parameter. In the local approach, two options can be considered. (i) The forbidden states can be those of the RGM [12,19,20]. (ii) They can also be "potential" forbidden states obtained by solving the local two-body equation with the considered potential [10,11]. In the local case, we consider both approaches. In the semi-microscopic model, only type (i) exists.

The method suggested by Kukulin *et al*. [9] consists in adding a pseudopotential to the three-body Hamiltonian H, i.e., the operator P multiplied by a large coefficient Λ [9]. Indeed, in a variational calculation of the expectation value

$$E^{J\pi} = \langle\Psi^{JM\pi}|H+\Lambda P|\Psi^{JM\pi}\rangle, \quad \Lambda\to\infty, \tag{23}$$

the large coefficient Λ leads to an elimination of the forbidden states.

C. Elimination method

Another procedure can be developed by considering the eigenvalues $\mu_\lambda^{J\pi}$ and eigenvectors $\Xi_\lambda^{JM\pi}$ of P,

$$P\,\Xi_\lambda^{JM\pi} = \mu_\lambda^{J\pi}\,\Xi_\lambda^{JM\pi}. \tag{24}$$

The eigenvalues are positive. Eliminating the two-body forbidden states is equivalent to using a subset of $\Xi_\lambda^{JM\pi}$ defined by

$$\mu_\lambda^{J\pi} = 0. \tag{25}$$

In practice, because the eigenvalues of Eq. (24) are obtained by using a finite basis, they are known approximately and Eq. (25) is replaced by

$$\mu_\lambda^{J\pi} \leqslant \mu_{\max}, \tag{26}$$

where $\mu_{\max}$ is close to zero.

Both methods of elimination are equivalent at the limit $\Lambda \to \infty$ because the eigenvalues $\mu_\lambda^{J\pi}$ are positive. They should give almost identical results in practical calculations if $\Lambda\langle P\rangle$ is negligible, as discussed below.

D. Comparisons within the local model

The conditions of the calculations will be detailed in Sec. V A. The present discussion is performed for the $\alpha\alpha n$ model of ^{9}Be. The $\alpha\alpha$ interaction [25] contains two forbidden states for $l = 0$ and one forbidden state for $l = 2$. The αn potential [29] contains one forbidden state for $l = 0$.

As explained above, we perform two types of comparison, i.e., between the projection and elimination techniques on the one hand and by using two types of two-body forbidden states on the other hand. The forbidden states are either consistent with the potential or taken as oscillator functions with some oscillator parameter b as in the RGM.

In Fig 1(a), we consider the ^{9}Be ground-state energy as a function of Λ (for $K_{\max} = 17$, see Sec. V A). Let us first discuss the pseudopotential method with $P^{\text{pot.}}$, i.e., with the exact two-body forbidden states of the corresponding potential (upper curve). The dotted line represents the energy after subtraction of $\Lambda\langle P\rangle$. A plateau is reached for $\Lambda \geqslant 10^6$ MeV but at a positive energy: the ground state is unbound with this pseudopotential. At smaller Λ values, the energies remain negative. This result contradicts the conclusion of Voronchev *et al.* [7], who find $E = -2.86$ MeV (we have checked that the difference of the αn potentials has virtually no effect). Most likely Voronchev *et al.* used a Λ value close to 1000 MeV.

In a second step, we use the harmonic oscillator functions as two-body forbidden states (with $b = 1.36$ and 1.40 fm). In that case the plateau corresponds to a bound ground state, with some sensitivity with respect to b: about 0.1 MeV for a very weak variation of b. The oscillator length b is a free parameter: it can be derived from the charge radius or from the variational principle for some potential. As there is no unique criterion to define the b value that should be used for the projection operator, this type of forbidden state may provide energies with an additional uncertainty.

In the elimination method, we first diagonalize the projection operator and use a limited basis (up to $\mu_\lambda^{J\pi} = \mu_{\max}$) to determine the ^{9}Be energy. The resulting ground-state energies are plotted in Fig. 1(b). As expected the converged values (i.e., $\mu_{\max} < 10^{-4}$) are identical to the converged values of Fig. 1(a). For the projector on the potential eigenstates, two regimes are clearly identified: at $E = +1.25$ MeV and at $E = -3.1$ MeV. The difference is due to a single eigenvalue 5.0×10^{-4} of the projection operator corresponding to an almost forbidden state [12]. According to whether this eigenvalue is included or not, two significantly different ^{9}Be energies can be obtained. The projection on harmonic-oscillator eigenstates also provides the same energies as the pseudopotential method.

The same techniques are applied in Fig. 2 to the $J = 5/2^-$ first excited state. The experimental energy is 0.86 MeV. With the potential eigenstates, the theoretical $5/2^-$ state is slightly bound, i.e., it is unrealistically below the $3/2^-$ state. The use of harmonic-oscillator functions in the projection operator also leads to a significant overbinding but yields reasonable

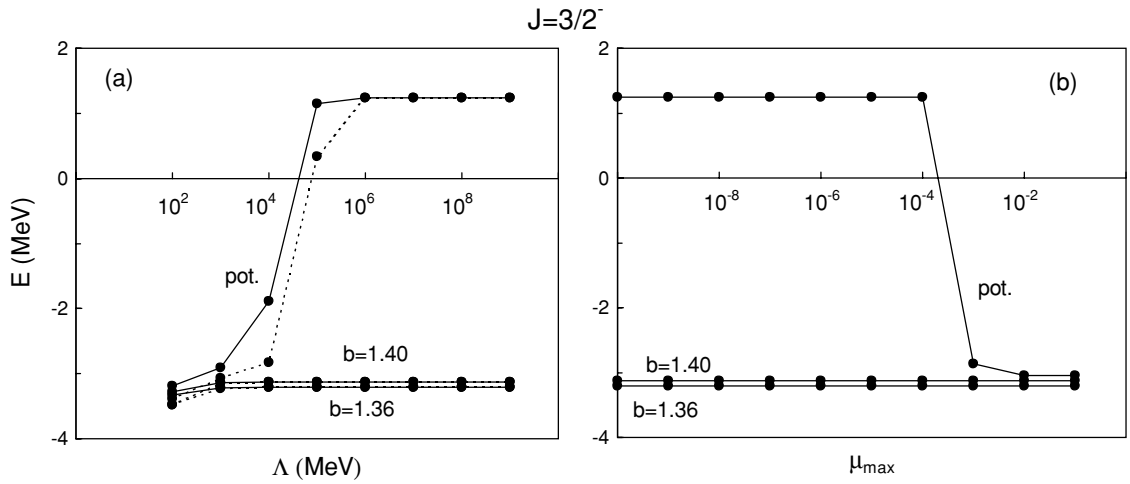

FIG. 1. Energy of the $3/2^-$ ground state in the local model calculated with the pseudopotential (a) and elimination (b) techniques. In each case, three operators are used: P^{pot} involving exact bound states of the two-body potentials, $P^{b=1.36}$ and $P^{b=1.40}$ involving harmonic-oscillator eigenstates with parameter $b/\sqrt{\mu_{ij}}$ (in fm). In (a), the full lines correspond to $\langle H + \Lambda P\rangle$ and the dotted lines to $\langle H\rangle$.

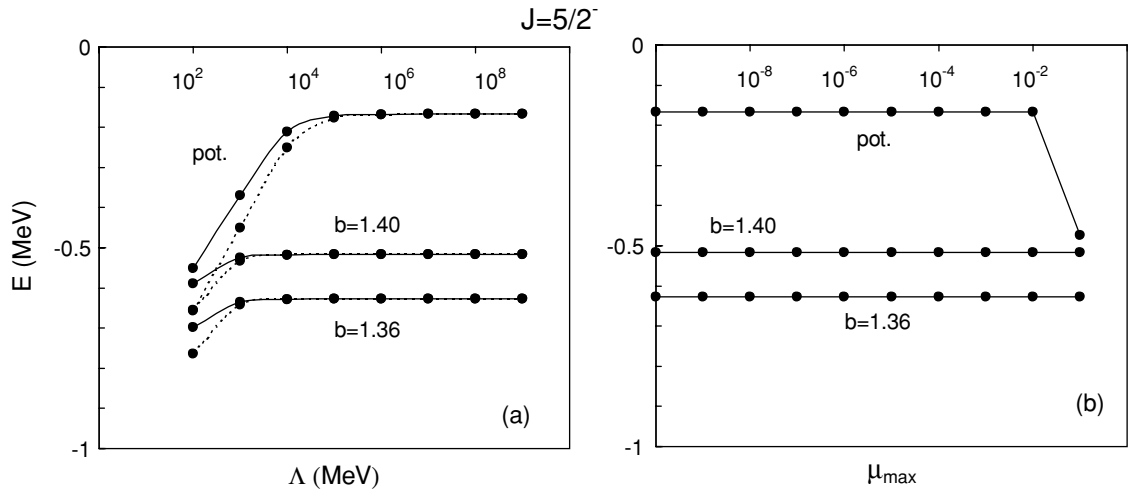

FIG. 2. See caption of Fig. 1 for the $5/2^-$ excited state.

^{9}Be($5/2^-$) excitation energies: 2.58 MeV for $b = 1.36$ fm and 2.61 MeV for $b = 1.40$ fm.

This type of result can be related to the apparent instability observed by Tursunov [10] for the ^{12}C ground state with $P^{\rm pot}$. Fitting the exact $\alpha\alpha$ forbidden states by a combination of Gaussian functions, Tursunov finds ^{12}C energies that are very sensitive to the size of the basis (see also Ref. [11]). As explained in Refs. [12,13], this instability is related to the presence or absence of two almost forbidden states with small nonvanishing eigenvalues $\mu_\lambda^{J\pi}$. The same effect is thus observed for the ^{9}Be case in Fig. 1.

E. Tests of semi-microscopic model calculations

Three-body calculations performed with the Faddeev method and using $\alpha\alpha$ RGM interactions are available for the $^9_\Lambda$Be hypernucleus and the ^{12}C nucleus in Ref. [20]. We carry out calculations under exactly the same conditions to test our results and in particular the validity of the forbidden-state removal.

The hypernucleus $^9_\Lambda$Be is modeled as an $\alpha\alpha\Lambda$ system with a nonlocal $\alpha\Lambda$ interaction whose expression in space coordinates can be found in Ref. [21]. The mass numbers are $A_\alpha = 4$ and $A_\Lambda = 1.18826$ in units of the nucleon mass m_N with $\hbar^2/2m_N = 20.7355$ MeV fm^2. The exchange parameter in the Minnesota force [30] is $u = 0.94687$ in the $\alpha\alpha$ interaction (see Sec. V A) and the α clusters correspond to $1/2b^2 = 0.257$ fm^{-2}. For $K_{\rm max} = 26$, the obtained ground-state energy $E = -6.838$ MeV and self-consistent value of parameter $\varepsilon_{\alpha\alpha} = 1.180$ MeV (see below) agree within 1 keV with Ref. [20]. We also perform a calculation of the 2^+ excited state for $K_{\rm max} = 20$ and obtain $E = -3.92$ MeV and $\varepsilon_{\alpha\alpha} = 4.02$ MeV also in excellent agreement with Ref. [20].

The ^{12}C nucleus is described as a system of three α clusters interacting with RGM nonlocal forces also under the same conditions as in Ref. [20] except that we treat the Coulomb interaction without any cutoff approximation. For $K_{\rm max} = 24$, we obtain the values $E = -9.599$ MeV and $\varepsilon_{\alpha\alpha} = 13.480$ MeV. The agreement with Ref. [20] is of about 5 keV on the ^{12}C energy.

V. COMPARISON OF MODELS FOR ^{9}Be AND ^{6}He

A. $\alpha\alpha$ and αn RGM potentials

The $\alpha\alpha$ and αn RGM potentials can be found in Appendix A, where they are adapted from Refs. [31,32]. The presentation differs because the exchange kernel depends here on the relative energy ε rather than on the total energy E_A.

The Minnesota nucleon-nucleon interaction [30] is employed both in the three-cluster microscopic model and in the derivation of the αn and $\alpha\alpha$ RGM potentials. Integer masses in units of the nucleon mass m_N are used in all cases. The value of m_N is fixed by $\hbar^2/2m_N = 20.736$ MeV fm^2. The internal wave functions (4) of the α clusters are chosen with a parameter $b = 1.36$ fm.

We take the value $u = 0.9474$ for the exchange parameter to get a good description of the $\alpha + \alpha$ phase shifts [33] (see Fig. 4 below). The RGM phase shifts are calculated with the Lagrange-mesh technique [34]. The αn RGM potential, including a spin-orbit term, is given in Appendix A as adapted from Ref. [32]. For the spin-orbit contribution, we define $\nu = 1/\sqrt{\lambda}$ and $S_0 = V_\lambda \nu^5$ [35]. In this way, we can choose $\nu = 0$ which has the nice property that the spin-orbit term becomes purely local in the RGM potential. With the u value selected for $\alpha + \alpha$, the choice $S_0 = 37$ MeV fm^5 reproduces the $\alpha + n$ phase shifts of Ref. [36] (see Fig. 3 below).

The $\alpha\alpha$ RGM potential generates two forbidden states for $l = 0$ and one forbidden state for $l = 2$. In the case of the αn RGM potential, there is one forbidden state, for $l = 0$.

Although an RGM potential is an effective interaction deduced from a microscopic model describing correctly the two-cluster system, it depends on the two-body energy ε that is not a constant of the motion in three-body systems. The values of ε must be fixed for each pair of clusters and become parameters. As suggested by Fujiwara *et al.* [19,20], a plausible prescription is to set these parameters equal to the

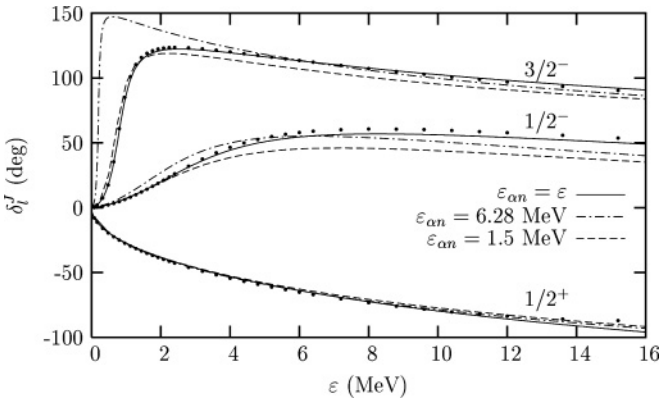

FIG. 3. $\alpha + n$ elastic phase shifts: RGM results (full lines) and nonlocal results with $\varepsilon_{\alpha n}$ fixed to its self-consistent value 6.28 MeV for ^{9}Be (dash-dotted lines) and the value 1.5 MeV reproducing the $p3/2$ and $p1/2$ resonances (dotted lines). Dots represent the phase shift analysis of Ref. [36].

mean energies of the two-body subsystems,

$$\varepsilon_{ij} = \langle \Psi^{JM\pi} | T_k + V_{ij} | \Psi^{JM\pi} \rangle, \tag{27}$$

where ε_{ij} is the parameter corresponding to V_{ij} and T_k is the kinetic energy of the relative motion between i and j (ijk being a circular permutation of the cluster indices 123). This leads to a self-consistent resolution of Eqs. (16) and (27). However, we show below that this choice of ε_{ij} is questionable and that another prescription is more appropriate in the present cases.

In addition, let us specify some technical parameters of the three-body model [8]. The sums over K in expansions (17) and (21) are truncated at some value $K_{\max}$. The hyperradial mesh is described with $N = 30$ mesh points and a scale parameter $h = 0.3$ fm for the ρ coordinate in Eq. (18). The nonlocal terms are calculated with $N_2 = 30$ mesh points and a scale parameter $h_2 = 0.08$ fm for the x Jacobi coordinate. Integrals over the y Jacobi coordinate are calculated with 800 points separated by a constant step 0.06 fm [see Eq. (B2)].

B. ^{9}Be nucleus as an $\alpha\alpha n$ system

The ^{9}Be nucleus is considered as a system of two α particles and a neutron. We study its $3/2^-$ ground state and $5/2^-$ excited state. We compare calculations within the local, semi-microscopic, and microscopic three-cluster models. The experimental values are -1.57 MeV for the ground-state energy with respect to the $\alpha\alpha n$ threshold and 2.43 MeV for the $5/2^-$ excitation energy [37].

We restrict the local model to its variant with oscillator forbidden states because the other variant leads to an unbound system for the experimental ground state and a bound system for the $5/2^-$ excited state. We focus on the oscillator parameter $b = 1.36$ fm, which reproduces the charge radius of the α particle. With the potentials of Refs. [25,29], the $3/2^-$ ground state of the ^{9}Be nucleus is overbound by about 1.5 MeV (see Fig. 1). The excitation energy of the $5/2^-$ state is close to experiment. In spite of the good quality of the effective forces for elastic scattering, this model fails to provide a good description of ^{9}Be.

TABLE I. Convergence of the $3/2^-$ and $5/2^-$ energies and of their difference ΔE (in MeV) of the $\alpha\alpha n$ system with respect to $K_{\max}$ within the semi-microscopic and microscopic models. The semi-microscopic $3/2^-$ energies are obtained with the self-consistent values $\varepsilon_{\alpha\alpha} = 3.61$ and $\varepsilon_{\alpha n} = 6.28$ MeV and the $5/2^-$ energies are obtained with the self-consistent values $\varepsilon_{\alpha\alpha} = 5.57$ and $\varepsilon_{\alpha n} = 6.39$ MeV [Eq. (27), see text].

$K_{\max}$	Semi-Microscopic			Microscopic		
	$3/2^-$	$5/2^-$	ΔE	$3/2^-$	$5/2^-$	ΔE
5	−1.64	0.87	2.50	−1.27	1.51	2.28
7	−2.39	0.17	2.55	−1.89	0.57	2.46
9	−3.41	−0.84	2.57	−2.23	0.22	2.46
11	−3.68	−1.11	2.57	−2.49	0.02	2.51
13	−3.79	−1.23	2.56	−2.55	−0.04	2.52
15	−3.83	−1.29	2.55	−2.60	−0.08	2.52
17	−3.85	−1.30	2.55	−2.61	−0.09	2.52
19	−3.86					

In fact the local model version that is the closest approximation to the semi-microscopic and microscopic models involves RGM direct potentials only, as defined in Eqs. (A3), (A4), and (A14). In this case the consistent forbidden states are obviously the harmonic-oscillator states. However, this model does not lead to a bound ^{9}Be system. The direct potentials, which are equivalent to double-folding potentials calculated with densities corresponding to Eq. (4), are less deep than the phenomenological potentials discussed above. The nonlocality of the interaction plays thus an essential role in binding the system within the RGM.

In the semi-microscopic model, also with $b = 1.36$ fm, the forbidden states are the same as in the local-model case just discussed. We start with prescription (27) for the parameters $\varepsilon_{\alpha\alpha}$ and $\varepsilon_{\alpha n}$ of the $\alpha\alpha$ and αn RGM interactions. The convergence of the energies as a function of $K_{\max}$ is presented in Table I. The values of the parameters $\varepsilon_{\alpha\alpha}$ and $\varepsilon_{\alpha n}$ are kept fixed in columns 2 and 3. They are consistent with the most accurate calculation (highest $K_{\max}$). A good convergence is obtained for $K_{\max} = 17$. The expectation value of the sum of nonlocal terms is as large as -7.80 MeV. This confirms that binding is not reached if nonlocality is neglected. Here also the ground state is overbound, by more than 2 MeV. However, the order of the $3/2^-$ and $5/2^-$ states is correct and the excitation energy is close to the experimental value 2.43 MeV.

To determine the reason of this overbinding, let us make a comparison with the microscopic model. The calculation is also performed with $b = 1.36$ fm and the same parameters for the Minnesota interaction. In the microscopic calculation, however, the $\alpha\alpha$ orbital angular momentum is limited to values $l_{\alpha\alpha} \leqslant 4$ [18]. If we apply the same restriction to the orbital angular momentum within the semi-microscopic model, the energy of the ground state becomes -3.83 MeV instead of -3.86 MeV for $K_{\max} = 19$. The restriction on $l_{\alpha\alpha}$ plays thus most probably a marginal role in the microscopic model.

The microscopic model also overestimates the binding of the α clusters and neutron but the overestimation is reduced

to about 1 MeV ($E = -2.61$ MeV, see Table I). Despite these differences, both models give the same excitation energy.

The larger overbinding in the semi-microscopic model leads us to reconsider the role of prescription (27). The αn interaction can be analyzed by looking at Fig. 3 which shows $\alpha + n$ elastic phase shifts. The curves $\varepsilon_{\alpha n} = \varepsilon$ correspond to the exact phase shifts within the RGM. They reproduce fairly well the phase-shift analysis of Ref. [36]. The other curves are obtained from the RGM potential with the energy ε replaced by a constant parameter $\varepsilon_{\alpha n} = 6.28$ MeV in the nonlocal kernel. They display the properties of the effective αn interaction that is actually used in the three-body system. Such an approximation is exact at the relative energy $\varepsilon = \varepsilon_{\alpha n}$ and thus most accurate around that energy. Within this fixed $\varepsilon_{\alpha n}$ approximation, the s-wave phase shift is good. However, the p-wave phase shifts and especially the $p3/2$ resonance are not well described with the self-consistent value of $\varepsilon_{\alpha n}$: the energy of the resonance is shifted down by about 0.8 MeV. The stronger overbinding of ^{9}Be in the semi-microscopic model is most probably related to this shift of the αn resonance. Rather than using prescription (27), it may be more efficient to use an $\varepsilon_{\alpha n}$ value reproducing the p-wave phase shifts as well as possible, such as $\varepsilon_{\alpha n} = 1.5$ MeV.

The situation is more satisfactory for the $\alpha\alpha$ RGM interaction. Figure 4 presents the $l = 0$ to 4 phase shifts for the $\alpha + \alpha$ elastic scattering. The effective $\alpha\alpha$ interaction in the three-body ^{9}Be system corresponds to $\varepsilon_{\alpha\alpha} = 3.61$ MeV. This value gives results rather close to the phase-shift analysis [33], except above an energy of 9 MeV for the $l = 4$ wave. It also affects the $l = 0$ resonance that is shifted to 0.5 MeV. The agreement is quite good around the $l = 2$ resonance. Other values of $\varepsilon_{\alpha\alpha}$ such as 2 or 6 MeV do not provide better results.

The self-consistent prescription (27), i.e., taking $\varepsilon_{\alpha\alpha}$ and $\varepsilon_{\alpha n}$ equal to the expectation value of the two-body energies, appears to be not well suited for the case of the ^{9}Be nucleus. Let us thus analyze the dependence of the $\alpha\alpha n$ ground-state energy on $\varepsilon_{\alpha\alpha}$ and $\varepsilon_{\alpha n}$. As shown in Fig. 5, this dependence is essentially linear with respect to both parameters $\varepsilon_{\alpha\alpha}$ and $\varepsilon_{\alpha n}$.

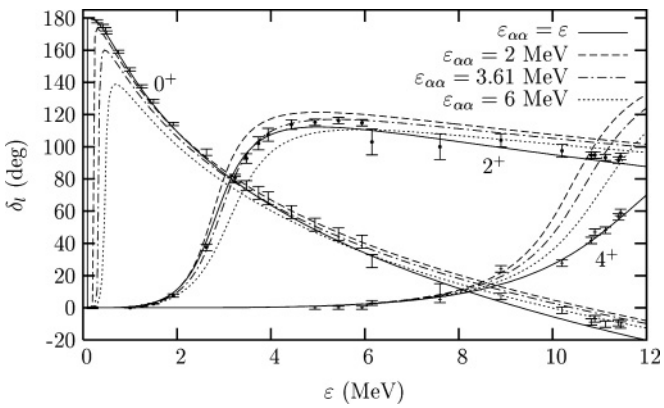

FIG. 4. $\alpha + \alpha$ elastic phase shifts: RGM results (full lines) and nonlocal results with $\varepsilon_{\alpha\alpha}$ fixed to its self-consistent value 3.61 MeV for ^{9}Be (dash-dotted lines) and two other values (dashed and dotted lines). Dots represent the phase shift analysis of Ref. [33].

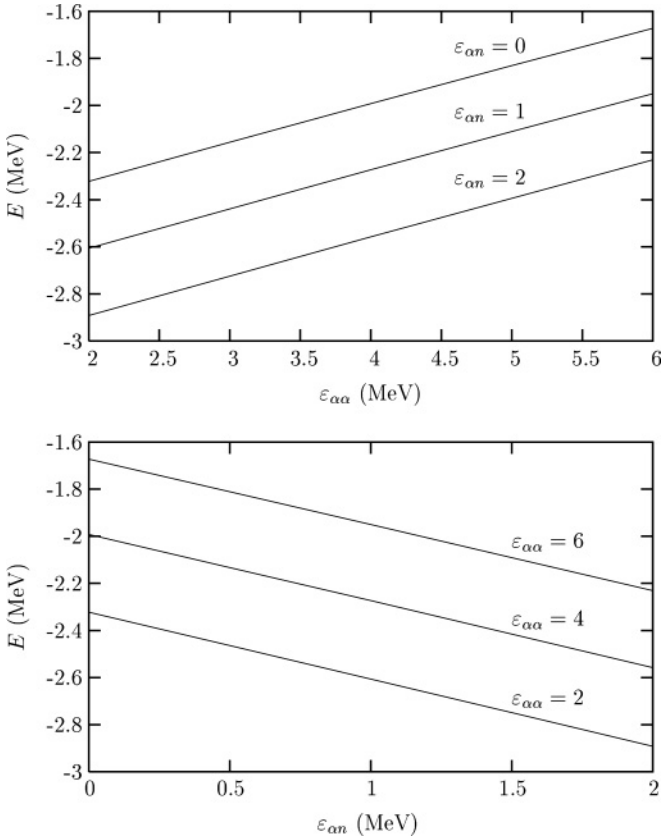

FIG. 5. Dependence on $\varepsilon_{\alpha\alpha}$ and $\varepsilon_{\alpha n}$ of the ground-state energy of ^{9}Be in the semi-microscopic model.

The curves in Fig. 5 can be fitted by

$$E \approx -2.64 + 0.16\,\varepsilon_{\alpha\alpha} - 0.28\,\varepsilon_{\alpha n} \qquad (28)$$

in MeV. Some $\alpha + \alpha$ and $\alpha + n$ phase shifts within the range of variation of the parameters are presented in Figs. 3 and 4. If one adopts the values of $\varepsilon_{\alpha\alpha}$ and $\varepsilon_{\alpha n}$ that give closer descriptions of the scattering experiments especially near the $\alpha + n$ $p3/2$ resonance, one obtains results similar to the energy -2.57 MeV of the microscopic three-cluster model. For example, with $\varepsilon_{\alpha\alpha} = 3.61$ MeV and $\varepsilon_{\alpha n} = 1.5$ MeV, the semi-microscopic model gives the energy $E = -2.48$ MeV. This means that three-body exchange effects have little importance in the microscopic calculation and that the semi-microscopic model reproduces its main physical properties.

Figure 5 suggests sets of $\varepsilon_{\alpha\alpha}$ and $\varepsilon_{\alpha n}$ reproducing the experimental energy of ^{9}Be but this procedure would not have much meaning. It leads to unrealistic choices of $\varepsilon_{\alpha\alpha}$ and $\varepsilon_{\alpha n}$ for the phase shifts.

The dependence of the $5/2^-$ energy on the parameters $\varepsilon_{\alpha\alpha}$ and $\varepsilon_{\alpha n}$ can be parametrized as

$$E \approx -0.42 + 0.16\,\varepsilon_{\alpha\alpha} - 0.28\,\varepsilon_{\alpha n} \qquad (29)$$

in MeV for $K_{\max} = 17$. Comparing with Eq. (28), one sees that the dependence is the same as for the ground state. Thus, the gap betwen the $3/2^-$ and $5/2^-$ levels for a given pair $(\varepsilon_{\alpha\alpha}, \varepsilon_{\alpha n})$ does not depend much on the values of this pair. This constant gap is about 2.22 MeV, i.e., somewhat smaller

than in the microscopic model. Notice that the gap is better in Table I because the parameters $\varepsilon_{\alpha n}$ and $\varepsilon_{\alpha\alpha}$ are different for each state.

The semi-microscopic and microscopic models essentially agree. They reproduce rather well the experimental excitation energy but overbind ^{9}Be. A common physical effect is missing.

C. ^{6}He nucleus as an αnn system

The ^{6}He nucleus has only one 0^+ bound state at -0.975 MeV with respect to the αnn threshold. It is described here as an α core and two halo neutrons. The local model for ^{6}He is discussed in Ref. [8] with the αn interaction of Ref. [29] and the nn Minnesota interaction (see Ref. [38] for other choices). The result obtained by projecting out the exact eigenstates of the αn potential [24] overestimates the ^{6}He energy (-0.42 MeV). The projection operator based on harmonic oscillator forbidden states does not lead here to significantly different results: -0.39 MeV for $b = 1.36$ fm and -0.40 MeV for $b = 1.40$ fm. Here also a local model based on the direct potential (A3) and (A4) does not bind ^{6}He.

The microscopic model is studied in Ref. [18] with the Minnesota interaction. Before discussing the results in that reference, we perform a calculation under the conditions of Sec. V A. For computing time reasons, we limit the hyperspherical-harmonics basis to $K_{\max} = 18$ and $l_{nn} \leqslant 4$ like in Ref. [18]. The effect of the l_{nn} limitation is marginal. The importance of the $K_{\max}$ truncation is estimated below. The microscopic model provides a very weak negative energy of -0.07 MeV.

Within the semi-microscopic model with the αn RGM potential explained in Sec. V A, the energy is -0.08 MeV for $K_{\max} = 28$ and the self-consistent value $\varepsilon_{\alpha n} = 1.65$ MeV. With a truncation at $K_{\max} = 18$ (but no l_{nn} restriction), the ^{6}He energy becomes -0.03 MeV in close agreement with the microscopic model. Because the difference is not large we keep $K_{\max} = 18$ in the following. The evolution of the energy with $\varepsilon_{\alpha n}$ is presented as the upper full curve in Fig. 6. If $\varepsilon_{\alpha n} < 1.5$ MeV, the three clusters are not bound.

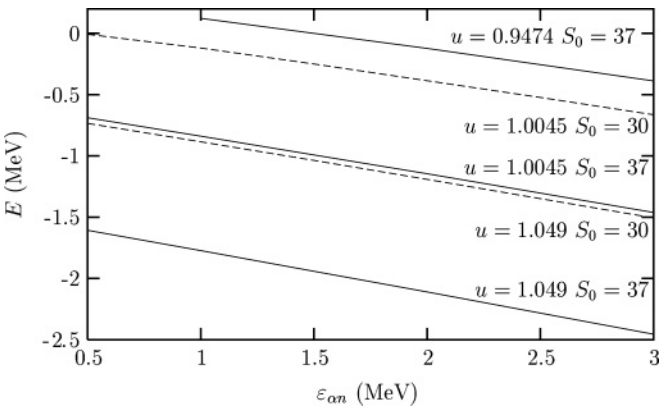

FIG. 6. Dependence on $\varepsilon_{\alpha n}$ of the energy of ^{6}He in the semi-microscopic model ($K_{\max} = 18$) for different combinations of the exchange parameter u of the Minnesota interaction and of the spin-orbit strength S_0 (in MeV fm^5).

In the microscopic model of Ref. [18], for a spin-orbit strength $S_0 = 30$ MeV fm^5, the exchange parameter is increased to the value $u = 1.049$ to reproduce the experimental value -0.975 MeV. It can also be reproduced for the present spin-orbit strength $S_0 = 37$ MeV fm^5 with $u = 1.0045$.

The roles of these changes can be analyzed within the semi-microscopic model for the truncation $K_{\max} = 18$. First let us consider the sensitivity on $\varepsilon_{\alpha n}$. The energy of ^{6}He as a function of this parameter is displayed in Fig. 6 for different cases considered for the microscopic calculation. As expected, the binding is stronger with $S_0 = 37$ MeV fm^5 than with $S_0 = 30$ MeV fm^5 for fixed u. Figure 6 shows that the experimental energy can be reproduced by setting $\varepsilon_{\alpha n} = 1.3$ MeV in the RGM potential for $S_0 = 30$ MeV fm^5 and $u = 1.049$. For $S_0 = 37$ MeV fm^5 and $u = 1.0045$, one needs $\varepsilon_{\alpha n} = 1.45$ MeV. Here also the nonlocality is essential for binding the system: the expectation value of both nonlocal αn potentials is for example -5.74 MeV in the latter case.

Now let us compare the microscopic and semi-microscopic models. We have learned from the ^{9}Be case the importance of the reproduction of phase shifts and, in particular, of the location of resonances. As shown in Fig. 7, the nucleon-nucleon interaction with the parameters $u = 1.049$ and $S_0 = 30$ MeV fm^5 does not provide a good description of the $\alpha + n$ scattering. This choice corresponds to the full curves $\varepsilon_{\alpha n} = \varepsilon$ in Fig. 7. It does not reproduce the experimental p-wave phase shifts. Let us fit $\varepsilon_{\alpha n}$ to the energy location obtained in the microscopic model for the $p3/2$ resonance. Figure 7 shows the effect of setting $\varepsilon_{\alpha n} = 0.5$ MeV in the αn RGM potential (dash-dotted curves). With this choice, the ^{6}He energy is -0.74 MeV. The same situation occurs for $u = 1.0045$ and $S_0 = 37$ MeV fm^5. The exact RGM (dashed curves) does not agree with experiment. If one reproduces the resonance location with $\varepsilon_{\alpha n} = 0.5$ MeV, one obtains -0.69 MeV. Because the $p1/2$ resonance is raised in better agreement with the data, the ^{6}He energy is here slightly higher.

In both cases, the semi-microscopic model is in fair agreement with the microscopic model when $\varepsilon_{\alpha n}$ is chosen

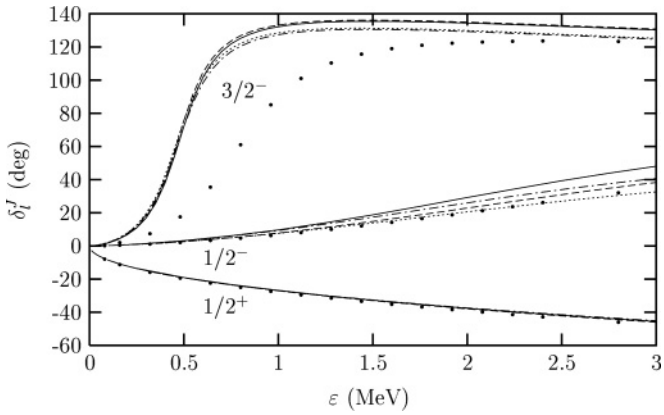

FIG. 7. $\alpha + n$ elastic phase shifts: RGM results (full lines for $u = 1.049$ and $S_0 = 30$ and dashed lines for $u = 1.0045$ and $S_0 = 37$) and semi-microscopic results with $\varepsilon_{\alpha n}$ fixed at 0.5 MeV so as to reproduce the RGM $p3/2$ resonance (dash-dotted lines for $u = 1.049$ and $S_0 = 30$ and dotted lines for $u = 1.0045$ and $S_0 = 37$). Dots represent the phase-shift analysis of Ref. [36].

in such a way that the $p3/2$ resonance is at the same energy. This means that three-body exchange effects are also weak here (0.25 or 0.3 MeV). The common feature of all these results is that the microscopic and semi-microscopic models can reproduce the experimental binding energy at the cost of an unrealistic energy location of the resonances that appear in the dominant p waves. The underestimation of the $p3/2$ resonance is about half the missing binding energy as intuitively expected. The fact that slightly better results are obtained here with the local model is thus probably somewhat fortuitous.

It is likely that the effective force with the increased u and/or S_0 values simulates the effect of three-nucleon forces. This interpretation is confirmed by Monte Carlo calculations with realistic forces that show that the contribution of the three-nucleon force is essential for a correct binding of ^{6}He [39]. Effective three-cluster forces would thus probably also be necessary to improve the semi-microscopic model. However, relating them to three-nucleon forces is probably not an easy task.

VI. CONCLUSION

The present work is devoted to a comparison of three different models, all based on the three-cluster physical picture and on the hyperspherical-coordinate formalism but otherwise rather different.

The local three-body model suffers from several drawbacks, i.e., the problem of choosing the cluster-cluster interactions and an ambiguity in the best definition of the forbidden states. It gives fair results for ^{6}He but poor results for ^{9}Be and ^{12}C. Because the local model is poorer than the other models for ^{9}Be and ^{12}C, its better success for ^{6}He is probably fortuitous. The local model as defined here remains useful when simplicity is the most important aspect. It is then better not to use deep cluster-cluster potentials involving forbidden states to avoid the complication and ambiguity introduced by their elimination.

The microscopic three-cluster model is well founded physically but requires high computing times to reach convergence. It provides a good qualitative description of ^{6}He, ^{9}Be, and ^{12}C, but binding energies are not very accurate or require tuning parameters. However, the tuned parameters are not consistent with scattering properties determined within the two-cluster RGM.

Between those models, the semi-microscopic model is better founded and more consistent than the local model and simpler than the microscopic model. Forbidden states must be eliminated but they are defined without ambiguity. This model contains a parameter in each cluster-cluster force whose choice appears to be delicate. The study of ^{9}Be indicates that the self-consistent prescription for the choice of parameter ε proposed by Fujiwara and coworkers [19] is not always satisfactory. A more physical prescription can be based on a fair reproduction of the phase shifts of the dominant partial waves, and in particular of their low-energy resonances. Anyway, this model can simulate the microscopic model as shown by both ^{6}He and ^{9}Be examples. Neglecting nucleon exchanges involving all three clusters does not lead to important errors.

The semi-microscopic model allows an interesting analysis of the microscopic model. The experimental binding energy is not reproduced with effective two-body forces that provide cluster-cluster RGM phase shifts in agreement with experiment. The binding energy is overestimated by about 1 MeV for ^{9}Be and underestimated by about 1 MeV in ^{6}He. The ^{6}He energy can be reproduced only if the energy of the $p3/2$ $\alpha + n$ resonance is underestimated by about half this amount. We think that the remaining discrepancy with experiment is due to a lack of three-nucleon forces.

ACKNOWLEDGMENTS

We thank Y. Fujiwara for providing us with tests and for interesting and lively discussions. This text presents research results of the Belgian program P5/07 on interuniversity attraction poles initiated by the Belgian-state Federal Services for Scientific, Technical and Cultural Affairs. M.T. is supported by a study grant from the Institut Interuniversitaire des Sciences Nucléaires (IISN), Belgium. P.D. acknowledges the support of the National Fund for Scientific Research (FNRS), Belgium.

APPENDIX A: αN AND αα RGM POTENTIALS

1. Nucleon-nucleon interaction

We assume a Gaussian nucleon-nucleon interaction of the form

$$V = V_0(W + BP_\sigma - HP_\tau - MP_\sigma P_\tau)\exp(-r^2/a^2). \quad \text{(A1)}$$

The spin-orbit NN interaction reads

$$V_{LS} = -2S_0\hbar^{-2}\nu^{-5}\exp(-r^2/\nu^2)\boldsymbol{L}\cdot\boldsymbol{S}. \quad \text{(A2)}$$

With this notation, a limit exists for ν tending to zero.

2. α + N system

For the sake of generality, we give here the $\alpha + p$ expression. For an oscillator parameter b, the central part of the direct potential reads

$$V_D(r) = \frac{1}{2}V_0X_d\left(\frac{4a^2}{4a^2+3b^2}\right)^{3/2} \times \exp\left(-\frac{4r^2}{4a^2+3b^2}\right) + \frac{2e^2}{r}\,\mathrm{erf}\left(\sqrt{\frac{4}{3b^2}}r\right), \quad \text{(A3)}$$

where the traditional notation $X_d = 8W + 4B - 4H - 2M$ and $X_e = 8M + 4H - 4B - 2W$ is introduced.

The spin-orbit part is given by

$$V_D^{LS}(r) = -\eta_l^J\frac{5}{2}S_0\left(\frac{4}{4\nu^2+3b^2}\right)^{5/2}\exp\left(-\frac{4r^2}{4\nu^2+3b^2}\right) \quad \text{(A4)}$$

with

$$\eta_l^J = J(J+1) - l(l+1) - S(S+1). \quad \text{(A5)}$$

Its zero-range limit is

$$V_D^{LS(0)} = -\eta_l^J \frac{5}{2} S_0 \left(\frac{4}{3b^2}\right)^{5/2} \exp\left(-\frac{4r^2}{3b^2}\right). \quad \text{(A6)}$$

The nonlocal potential is separated in several terms,

$$K = K_T + K_V + K_{LS} + K_C + \varepsilon K_N. \quad \text{(A7)}$$

The overlap kernel is given by

$$K_N(\boldsymbol{r}, \boldsymbol{r}') = \left(\frac{4}{5}\right)^3 \left(\frac{4}{3\pi b^2}\right)^{3/2} \times \exp\left[-\frac{2}{75b^2}(17r^2 + 17r'^2 + 16\boldsymbol{r}\cdot\boldsymbol{r}')\right]. \quad \text{(A8)}$$

The kinetic-energy kernel is given by

$$K_T(\boldsymbol{r}, \boldsymbol{r}') = -\frac{1}{4}\hbar\omega \left[\frac{49}{5} - \frac{64}{1125b^2} \times (38r^2 + 38r'^2 + 49\boldsymbol{r}\cdot\boldsymbol{r}')\right] K_N. \quad \text{(A9)}$$

The central nuclear potential kernel is given by

$$K_V(\boldsymbol{r}, \boldsymbol{r}') = \frac{1}{2} V_0 \left((X_d + X_e) \left(\frac{a^2}{a^2 + 2b^2}\right)^{3/2} + X_e \exp\left[-\frac{16(\boldsymbol{r} - \boldsymbol{r}')^2}{25a^2}\right] - (X_d + X_e) \left(\frac{3a^2}{3a^2 + 2b^2}\right)^{3/2} \times \left\{ \exp\left[-\frac{16(4\boldsymbol{r} + \boldsymbol{r}')^2}{75(3a^2 + 2b^2)}\right] + \exp\left[-\frac{16(\boldsymbol{r} + 4\boldsymbol{r}')^2}{75(3a^2 + 2b^2)}\right] \right\} \right) K_N. \quad \text{(A10)}$$

The spin-orbit kernel reads

$$K_{LS}(\boldsymbol{r}, \boldsymbol{r}') = -\eta_{lj} S_0 \nu^{-3} \frac{5}{3b^2 - \nu^2} \exp\left[-\frac{16(\boldsymbol{r} - \boldsymbol{r}')^2}{25\nu^2}\right] K_N. \quad \text{(A11)}$$

Its zero-range limit is local,

$$K_{LS}^{(0)}(\boldsymbol{r}, \boldsymbol{r}') = \tfrac{1}{2} V_D^{LS(0)}(r) \delta(\boldsymbol{r} - \boldsymbol{r}'). \quad \text{(A12)}$$

The Coulomb kernel is given by

$$K_C(\boldsymbol{r}, \boldsymbol{r}') = e^2 \left\{ \frac{2^{1/2}}{\pi^{1/2} b} - \frac{5}{4|\boldsymbol{r} - \boldsymbol{r}'|} - \frac{15}{4} \left[\frac{\operatorname{erf}\left(\frac{4}{5}\sqrt{\frac{1}{6b^2}}|4\boldsymbol{r} + \boldsymbol{r}'|\right)}{|4\boldsymbol{r} + \boldsymbol{r}'|} + \frac{\operatorname{erf}\left(\frac{4}{5}\sqrt{\frac{1}{6b^2}}|\boldsymbol{r} + 4\boldsymbol{r}'|\right)}{|\boldsymbol{r} + 4\boldsymbol{r}'|} \right] \right\} K_N. \quad \text{(A13)}$$

3. $\alpha + \alpha$ system

The central part of the direct potential reads

$$V_D(r) = 2V_0 X_d \left(\frac{2a^2}{2a^2 + 3b^2}\right)^{3/2} \times \exp\left(-\frac{2r^2}{2a^2 + 3b^2}\right) + \frac{4e^2}{r} \operatorname{erf}\left(\sqrt{\frac{2}{3}}\frac{r}{b}\right). \quad \text{(A14)}$$

Spin-orbit terms vanish.

The $\alpha + \alpha$ kernels are symmetric with respect to $\boldsymbol{r}' \to -\boldsymbol{r}'$. They are given below in unsymmetrized form, i.e.,

$$K(\boldsymbol{r}, \boldsymbol{r}') = \tfrac{1}{2}[K^{(u)}(\boldsymbol{r}, \boldsymbol{r}') + K^{(u)}(\boldsymbol{r}, -\boldsymbol{r}')] \quad \text{(A15)}$$

for each type of kernel. The unsymmetrized expressions $K^{(u)}(\boldsymbol{r}, \boldsymbol{r}')$ directly lead to the correct projected kernels provided only even l values are kept. Odd l values are forbidden.

The norm kernel reads

$$K_N^{(u)}(\boldsymbol{r}, \boldsymbol{r}') = 4\left(\frac{8}{3\pi b^2}\right)^{3/2} \exp\left(-\frac{5r^2 + 5r'^2 - 8\boldsymbol{r}\cdot\boldsymbol{r}'}{3b^2}\right) - 3\left(\frac{2}{\pi b^2}\right)^{3/2} \exp\left(-\frac{r^2 + r'^2}{b^2}\right). \quad \text{(A16)}$$

The kinetic-energy kernel is given by

$$K_T^{(u)}(\boldsymbol{r}, \boldsymbol{r}') = -\hbar\omega \left\{ \left(\frac{8}{3\pi b^2}\right)^{3/2} \times \left[13 - \frac{112(r^2 + r'^2) - 208\boldsymbol{r}\cdot\boldsymbol{r}'}{9b^2}\right] \times \exp\left(-\frac{5r^2 + 5r'^2 - 8\boldsymbol{r}\cdot\boldsymbol{r}'}{3b^2}\right) - \left(\frac{2}{\pi b^2}\right)^{3/2} \times \left(\frac{27}{4} - 3\frac{r^2 + r'^2}{b^2}\right) \exp\left(-\frac{r^2 + r'^2}{b^2}\right) \right\}. \quad \text{(A17)}$$

The central nuclear potential kernel is given by

$$K_V^{(u)}(\boldsymbol{r}, \boldsymbol{r}') = V_0 \left(\frac{8}{3\pi b^2}\right)^{3/2} \exp\left(-\frac{5r^2 + 5r'^2 - 8\boldsymbol{r}\cdot\boldsymbol{r}'}{3b^2}\right) \times \left\{ 4(X_d + X_e) \left(\frac{a^2}{a^2 + 2b^2}\right)^{3/2} + 2X_e \exp\left[-\frac{4(\boldsymbol{r} - \boldsymbol{r}')^2}{a^2}\right] - 2(2X_d - X_e) \times \left(\frac{3a^2}{3a^2 + 4b^2}\right)^{3/2} \exp\left[-\frac{4(\boldsymbol{r} + \boldsymbol{r}')^2}{3(3a^2 + 4b^2)}\right] - 4(X_d + X_e) \left(\frac{3a^2}{3a^2 + 4b^2}\right)^{3/2} \times \left\{ \exp\left[-\frac{4(2\boldsymbol{r} - \boldsymbol{r}')^2}{3(3a^2 + 4b^2)}\right] + \exp\left[-\frac{4(\boldsymbol{r} - 2\boldsymbol{r}')^2}{3(3a^2 + 4b^2)}\right] \right\}$$

$$+V_0\left(\frac{2}{\pi b^2}\right)^{3/2}\exp\left(-\frac{r^2+r'^2}{b^2}\right)$$
$$\times\left\{2(X_d-2X_e)\left(\frac{a^2}{a^2+b^2}\right)^{3/2}\right.$$
$$\times\exp\left[-\frac{(\boldsymbol{r}-\boldsymbol{r}')^2}{a^2+b^2}\right]-4(X_d+X_e)$$
$$\times\left(\frac{a^2}{a^2+2b^2}\right)^{3/2}+4(X_d+X_e)\left(\frac{2a^2}{2a^2+3b^2}\right)^{3/2}$$
$$\left.\times\left[\exp\left(-\frac{2r^2}{2a^2+3b^2}\right)+\exp\left(-\frac{2r'^2}{2a^2+3b^2}\right)\right]\right\}. \quad \text{(A18)}$$

The Coulomb kernel reads

$$K_C^{(u)}(\boldsymbol{r},\boldsymbol{r}')=e^2\left(\frac{8}{3\pi b^2}\right)^{3/2}\exp\left(-\frac{r^2+r'^2}{3b^2}\right)$$
$$\times\exp\left(-\frac{4(\boldsymbol{r}-\boldsymbol{r}')^2}{3b^2}\right)\left[4\left(\frac{2}{\pi b^2}\right)^{1/2}\right.$$
$$-\frac{1}{|\boldsymbol{r}-\boldsymbol{r}'|}-15\frac{\mathrm{erf}\left(\frac{1}{\sqrt{3}b}|\boldsymbol{r}+\boldsymbol{r}'|\right)}{|\boldsymbol{r}+\boldsymbol{r}'|}$$
$$\left.-6\frac{\mathrm{erf}\left(\frac{1}{\sqrt{3}b}|2\boldsymbol{r}-\boldsymbol{r}'|\right)}{|2\boldsymbol{r}-\boldsymbol{r}'|}-6\frac{\mathrm{erf}\left(\frac{1}{\sqrt{3}b}|\boldsymbol{r}-2\boldsymbol{r}'|\right)}{|\boldsymbol{r}-2\boldsymbol{r}'|}\right]$$
$$+4e^2\left(\frac{2}{\pi b^2}\right)^{3/2}\exp\left(-\frac{r^2+r'^2}{b^2}\right)$$
$$\times\left[2\frac{\mathrm{erf}\left(\frac{1}{b}|\boldsymbol{r}-\boldsymbol{r}'|\right)}{|\boldsymbol{r}-\boldsymbol{r}'|}-\left(\frac{2}{\pi b^2}\right)^{1/2}\right.$$
$$\left.+\frac{\mathrm{erf}\left(\frac{\sqrt{2}r}{\sqrt{3}b}\right)}{r}+\frac{\mathrm{erf}\left(\frac{\sqrt{2}r'}{\sqrt{3}b}\right)}{r'}\right]. \quad \text{(A19)}$$

4. Projection on orbital momentum

Projected kernels are given by

$$k_l(r,r')=2\pi rr'\int_{-1}^{+1}K(\boldsymbol{r},\boldsymbol{r}')P_l(u)\,du \quad \text{(A20)}$$

with $u=\cos\theta$, where θ is the angle between $\boldsymbol{r}$ and $\boldsymbol{r}'$.

Some terms can be expanded analytically in a simple way. Exponential terms can be calculated with

$$\exp(\alpha\boldsymbol{r}\cdot\boldsymbol{r}')=\sum_{l=0}^{\infty}(2l+1)P_l(\cos\theta)i_l(\alpha rr'), \quad \text{(A21)}$$

where i_l is a modified spherical Bessel function or spherical Hankel function, i.e.,

$$\int_{-1}^{+1}\exp(\pm|\alpha|\boldsymbol{r}\cdot\boldsymbol{r}')P_l(u)du=2(\pm1)^l i_l(|\alpha|rr'). \quad \text{(A22)}$$

Coulomb terms can be calculated with

$$\int_{-1}^{+1}\frac{1}{|\boldsymbol{r}\pm\boldsymbol{r}'|}P_l(u)\,du=(\mp1)^l\frac{2}{2l+1}\frac{r_<^l}{r_>^{l+1}} \quad \text{(A23)}$$

where $r_>=\max(r_1,r_2)$ and $r_<=\min(r_1,r_2)$. Screened Coulomb terms

$$\int_{-1}^{+1}\frac{f(|\boldsymbol{r}\pm\boldsymbol{r}'|)}{|\boldsymbol{r}\pm\boldsymbol{r}'|}P_l(u)\,du$$
$$=\frac{(\pm1)^l}{r_>}\int_{-1}^{+1}f(r_>+vr_<)P_l\left[v-(1-v^2)\frac{r_<}{2r_>}\right]dv \quad \text{(A24)}$$

require a numerical integration that can be performed accurately with a Gauss-Legendre quadrature.

APPENDIX B: CALCULATION OF THE TWO-BODY ENERGIES

Each RGM potential depends on the energy of the system made up by the two interacting clusters. In this Appendix, the numerical evaluation of the mean energy (27) is presented in the hyperspherical-coordinate system. We adopt the same notation as in Refs. [8,21] where definitions can be found.

The expectation value of the potential energy V_{ij} can be directly calculated with

$$\langle\Psi^{JM\pi}|V_{ij}|\Psi^{JM\pi}\rangle$$
$$=\sum_{\gamma Ki\,\gamma'K'i'}\left[V^{J\pi(k)}_{\gamma K,\gamma'K'}(hu_i)\delta_{ii'}+W^{J\pi(k)}_{\gamma Ki,\gamma'K'i'}\right]C^{J\pi}_{\gamma Ki}C^{J\pi}_{\gamma'K'i'} \quad \text{(B1)}$$

from the matrix elements $V^{J\pi}_{\gamma K,\gamma'K'}$ and $W^{J\pi}_{\gamma Ki,\gamma'K'i'}$ of Refs. [8,21]. The calculation of the kinetic energy is performed from

$$\langle\Psi^{JM\pi}|T_k|\Psi^{JM\pi}\rangle$$
$$=\frac{\hbar^2}{2m_N}\sum_{\gamma KK'}\left[\int_0^\infty y^2dy\int_0^\infty\frac{\partial}{\partial x}\left(\frac{x\phi_K^{l_xl_y}\chi^{J\pi}_{\gamma K}}{\rho^{5/2}}\right)\right.$$
$$\times\frac{\partial}{\partial x}\left(\frac{x\phi_{K'}^{l_xl_y}\chi^{J\pi}_{\gamma K'}}{\rho^{5/2}}\right)dx+l_x(l_x+1)$$
$$\left.\times\int_0^{\frac{\pi}{2}}\sin^2\alpha\phi_K^{l_xl_y}\phi_{K'}^{l_xl_y}\,d\alpha\int_0^\infty\frac{\chi^{J\pi}_{\gamma K}\chi^{J\pi}_{\gamma K'}}{\rho^2}d\rho\right], \quad \text{(B2)}$$

where $\phi_K^{l_xl_y}$ is defined by Eq. (9) of Ref. [8] and x and y are scaled Jacobi coordinates. Using expansion (18) of functions $\chi^{J\pi}_{\gamma K}$ in the Lagrange basis, one obtains

$$\langle\Psi^{JM\pi}|T_k|\Psi^{JM\pi}\rangle=\frac{\hbar^2}{2m_Nh^2}\sum_{\gamma KK'ii'}\left[\frac{1}{u_i^2}\left(\frac{15}{2}\delta_{KK'}-\frac{45}{4}B_{\gamma KK'}\right.\right.$$
$$\left.+E_{\gamma KK'}+l_x(l_x+1)A_{\gamma KK'}\right)\delta_{ii'}$$
$$\left.+\hat{T}_{ii'}B_{\gamma KK'}-2U_{ii'}D_{\gamma KK'}\right]C^{J\pi}_{\gamma Ki}C^{J\pi}_{\gamma K'i'}, \quad \text{(B3)}$$

where

$$A_{\gamma KK'} = \int_0^{\frac{\pi}{2}} \sin^2\alpha \phi_K^{l_x l_y} \phi_{K'}^{l_x l_y} d\alpha, \tag{B4}$$

$$B_{\gamma KK'} = \int_0^{\frac{\pi}{2}} \sin^2\alpha \cos^4\alpha \phi_K^{l_x l_y} \phi_{K'}^{l_x l_y} d\alpha, \tag{B5}$$

$$D_{\gamma KK'} = \int_0^{\frac{\pi}{2}} \sin^3\alpha \cos^3\alpha \frac{d\phi_K^{l_x l_y}}{d\alpha} \phi_{K'}^{l_x l_y} d\alpha, \tag{B6}$$

$$E_{\gamma KK'} = \int_0^{\frac{\pi}{2}} \sin^4\alpha \cos^2\alpha \frac{d\phi_K^{l_x l_y}}{d\alpha} \frac{d\phi_{K'}^{l_x l_y}}{d\alpha} d\alpha, \tag{B7}$$

and

$$\hat{T}_{ii'} = -\int_0^\infty \hat{f}_i(u) \frac{d^2 \hat{f}_{i'}(u)}{du^2} du, \tag{B8}$$

$$U_{ii'} = \int_0^\infty \hat{f}_i(u) \frac{1}{u} \frac{d\hat{f}_{i'}(u)}{du} du. \tag{B9}$$

The matrix elements $\hat{T}_{ii'}$ and $U_{ii'}$ are evaluated with the Gauss-Laguerre quadrature. The expressions for $T_{ii'}$ are given in Eqs. (32) and (33) of Ref. [8] the phase in Eq. (33) is misprinted and should be $(-1)^{i+i'+1}$]. The other matrix elements read

$$U_{ii'} \approx \frac{\lambda_i^{1/2} \hat{f}'_{i'}(u_i)}{u_i} = \begin{cases} \frac{1}{2u_i^2} & \text{if } i = i', \\ \frac{(-1)^{i+i'}}{2u_{i'}(u_i - u'_i)} & \text{if } i \neq i. \end{cases} \tag{B10}$$

The integrals $B_{\gamma KK'}$ and $D_{\gamma KK'}$ are evaluated with the help of properties of the Jacobi polynomials [40] as

$$B_{\gamma KK'} = \begin{cases} \frac{1}{2(K+2)} \sqrt{\frac{n(n+l_x+l_y+1)(2n+2l_x+1)(2n+2l_y+1)}{K(K+2)}} \\ \quad \text{if } n' = n-1 \\ \frac{1}{2}\left(1 + \frac{(l_x+l_y+1)(l_x-l_y)}{(K+1)(K+3)}\right) \\ \quad \text{if } n' = n \\ \frac{1}{2(K+3)} \sqrt{\frac{(n+1)(n+l_x+l_y+2)(2n+2l_x+3)(2n+2l_y+3)}{(K+2)(K+4)}} \\ \quad \text{if } n' = n+1 \\ 0 \qquad \text{otherwise} \end{cases} \tag{B11}$$

$$D_{\gamma KK'} = \begin{cases} -\frac{K+4}{2(K+1)} \sqrt{\frac{n(n+l_x+l_y+1)(2n+2l_x+1)(2n+2l_y+1)}{K(K+2)}} \\ \quad \text{if } n' = n-1 \\ \frac{3(l_x+l_y+1)(l_y-l_x)}{2(K+1)(K+3)} \\ \quad \text{if } n' = n \\ \frac{K}{2(K+3)} \sqrt{\frac{(n+1)(n+l_x+l_y+2)(2n+2l_x+3)(2n+2l_y+3)}{(K+2)(K+4)}} \\ \quad \text{if } n' = n+1 \\ 0 \qquad \text{otherwise.} \end{cases} \tag{B12}$$

where $n = (K - l_x - l_y)/2$ and $n' = (K' - l_x - l_y)/2$. The integration over α in $A_{\gamma KK'}$ and $E_{\gamma KK'}$ is performed numerically.

[1] K. Wildermuth and Y. C. Tang, *A Unified Theory of the Nucleus* (Vieweg, Braunschweig, 1977).
[2] S. Saito, Prog. Theor. Phys. Suppl. **62**, 11 (1977).
[3] Y. Fujiwara, H. Horiuchi, K. Ikeda, M. Kamimura, K. Katō, Y. Suzuki, and E. Uegaki, Prog. Theor. Phys. Suppl. **68**, 29 (1980).
[4] J. L. Visschers and R. Van Wageningen, Phys. Lett. **34B**, 455 (1971).
[5] R. M. Mendez-Moreno, M. Moreno, and T. Seligman, Nucl. Phys. **A221**, 381 (1974).
[6] Y. F. Smirnov, I. T. Obukhovsky, Y. M. Tchuvil'sky, and V. G. Neudatchin, Nucl. Phys. **A235**, 289 (1974).
[7] V. T. Voronchev, V. I. Kukulin, V. N. Pomerantsev, and G. G. Ryzhikh, Few-Body Syst. **18**, 191 (1995).
[8] P. Descouvemont, C. Daniel, and D. Baye, Phys. Rev. C **67**, 044309 (2003).
[9] V. I. Kukulin and V. N. Pomerantsev, Ann. Phys. (NY) **111**, 330 (1978).
[10] E. M. Tursunov, J. Phys. G **27**, 1381 (2001).
[11] E. M. Tursunov, D. Baye, and P. Descouvemont, Nucl. Phys. **A723**, 365 (2003).
[12] Y. Fujiwara, Y. Suzuki, and M. Kohno, Phys. Rev. C **69**, 037002 (2004).
[13] H. Matsumura, M. Orabi, Y. Suzuki, and Y. Fujiwara, Nucl. Phys. **A776**, 1 (2006).
[14] M. Kamimura, Nucl. Phys. **A351**, 456 (1981).
[15] P. Descouvemont and D. Baye, Phys. Rev. C **36**, 54 (1987).
[16] P. Descouvemont, Phys. Rev. C **52**, 704 (1995).
[17] Y. Suzuki and K. Varga, *Stochastic Variational Approach to Quantum-Mechanical Few-Body Problems* (Springer, Berlin, 1998).
[18] S. Korennov and P. Descouvemont, Nucl. Phys. **A740**, 249 (2004).
[19] Y. Fujiwara, Y. Suzuki, K. Miyagawa, M. Kohno, and H. Nemura, Prog. Theor. Phys. **107**, 993 (2002).
[20] Y. Fujiwara, K. Miyagawa, M. Kohno, Y. Suzuki, D. Baye, and J.-M. Sparenberg, Phys. Rev. C **70**, 024002 (2004).
[21] M. Theeten, D. Baye, and P. Descouvemont, Nucl. Phys. **A753**, 233 (2005).
[22] D. Baye and P.-H. Heenen, J. Phys. A **19**, 2041 (1986).
[23] D. Baye, M. Hesse, and M. Vincke, Phys. Rev. E **65**, 026701 (2002).
[24] P. Descouvemont, E. M. Tursunov, and D. Baye, Nucl. Phys. **A765**, 370 (2006).
[25] B. Buck, H. Friedrich, and C. Wheatley, Nucl. Phys. **A275**, 246 (1977).
[26] E. W. Schmid, Z. Phys. A **302**, 311 (1981).
[27] Y. Suzuki, R. G. Lovas, K. Yabana, and K. Varga, *Structure and Reactions of Light Exotic Nuclei* (Taylor & Francis, London, 2003).
[28] S. Nakaichi-Maeda and E. W. Schmid, Z. Phys. A **318**, 171 (1984).
[29] H. Kanada, T. Kaneko, S. Nagata, and M. Nomoto, Prog. Theor. Phys. **61**, 1327 (1979).
[30] D. R. Thomson, M. LeMere, and Y. C. Tang, Nucl. Phys. **A286**, 53 (1977).
[31] D. R. Thompson, I. Reichstein, W. McClure, and Y. C. Tang, Phys. Rev. **185**, 1351 (1969).
[32] I. Reichstein and Y. C. Tang, Nucl. Phys. **A158**, 529 (1970).
[33] S. A. Afzal, A. Ahmed, and S. Ali, Rev. Mod. Phys. **41**, 247 (1969).

[34] M. Hesse, J. Roland, and D. Baye, Nucl. Phys. **A709**, 184 (2002).
[35] D. Baye and N. Pecher, Bull. Cl. Sc. Acad. Roy. Belg. **67**, 835 (1981).
[36] G. L. Morgan and R. L. Walter , Phys. Rev. **168**, 1114 (1968).
[37] R. B. Firestone and V. S. Shirley, *Table of Isotopes* (Wiley, New York, 1996).
[38] E. M. Tursunov, D. Baye, and P. Descouvemont, Phys. Rev. C **73**, 014303 (2006).
[39] S. C. Pieper, R. B. Wiringa, and J. Carlson, Phys. Rev. C **70**, 054325 (2004).
[40] I. S. Gradshteyn and I. M. Ryzhik, *Table of Integrals, Series, and Products* (Academic, New York, 1980).